Flexural performance of concrete slabs reinforced with GFRP rebars

O. Elzaroug[1], J. Forth[2], J. YE[3] and A. Beeby[2]
[1]Omar El-Mukhtar University, Civil Engineering Department, Elbeida, Libya
[2]University of Leeds, School of Civil Engineering, Leeds, UK
[3]Lancaster University, Department of Engineering, Lancaster, UK

Abstract. The use of non-metallic fibre reinforced polymer (FRP) reinforcement as an alternative to steel reinforcement in concrete is gaining acceptance mainly due to its high corrosion resistance. High strength-to-weight ratio, high stiffness-to-weight ratio and ease of handling and fabrication are added advantages. Other benefits are that they do not influence to magnetic fields and radio frequencies and they are thermally non-conductive. However, the stress-strain relationship for Glass FRP is linear up to rupture when the ultimate strength is reached. Unlike steel reinforcing bars, GFRP rebars do not undergo yield deformation or strain hardening before rupture. Also, GFRP reinforcement possesses a relatively low elastic modulus of elasticity compared with that of steel. As a consequence, for GFRP reinforced sections, larger deflections and crack widths are expected than the ones obtained from equivalent steel reinforced sections for the same load. This paper presents a comparison of the experimental results with those predicted by the ACI 440 code in terms of; measured cracking moment, load-deflection relationships, ultimate capacity, modes of failure, stresses and crack width. This is to investigate the suitability of using the existing ACI design equations for predicting the flexural behaviour of samples reinforced with GFRP rebars. In this investigation, it appears that the ACI code equations on the whole over predict (i.e. crack widths and midspan deflection) the experimental results. On the other hand, the maximum experimental moment satisfies the ACI condition (i.e. unfactored design moment).

1 Introduction

The flexural design of concrete sections reinforced with Glass FRP (GFRP) is different from that of sections reinforced with steel because of the difference in mechanical properties of GFRP and steel. Generally, the GFRP bars used as reinforcement in concrete have tensile strengths varying between 620 and 690 MPa and a modulus of elasticity of around 40 GPa [1]. The tensile strength varies as the diameter of the bar increases due to shear lag which develops between the fibers in the larger sizes. The stress-strain relationship for GFRP is linear up to rupture when the ultimate strength is reached. Unlike steel reinforcing bars, GFRP rebars do not undergo yield deformation or strain hardening before rupture. For this reason, the flexural design of sections reinforced with GFRP has been based on: (i) ultimate strength, (ii) serviceability (the low elasticity modulus of GFRP shifts the design criteria to the serviceability limit states that check the structural behaviour aspect instead of the strength to assure functionality and safety during its life), (iii) shear and (iv) deformability (the deformability factor is defined as the product ratio of moment multiplied by curvature at ultimate failure and at serviceability [2]. For steel reinforced sections, the cross section of steel is commonly governed by the ultimate strength requirement. There are, however, some cases where the design is governed by the need to control crack width in service (e.g. water retaining structures).

GFRP reinforced concrete members have a relatively low stiffness after cracking. Consequently, the permissible deflection under service loads can control the design. In general, designing GFRP reinforced cross sections for concrete crushing failure satisfies the serviceability criteria for deflection and crack width [2]. Deflections in ACI 440 [2] are calculated based on an effective second moment of area, I_e (Eq. 1).

$$I_e = (M_{cr}/M_a)^3 \beta_d I_g + [1 - (M_{cr}/M_a)^3] I_{cr} \leq I_g \quad (1)$$

$$\beta_d = (\rho_f / 5\rho_{fb}) \leq 1.0 \quad (2)$$

Where I_{cr} is the cracked second moment of area, mm^4; I_g is the gross second moment of area, mm^4; M_a is the applied moment, N mm; M_{cr} is the cracking moment, N mm; β_d is the reduction coefficient related to the reduced tension stiffening exhibited by FRP-reinforced members; ρ_f is the FRP reinforcement ratio; and ρ_{fb} is the balanced reinforcement ratio of FRP rods.

However, Ospina and Nanni [3] stated that the term β_d in equation (1) which is dependent on ρ_{bf} is conceptually incorrect. This is because it would imply that different deflections can be predicted for members reinforced with FRP bars that have similar stiffness but different ultimate tensile strength, f_{fu}. Since deflection is a problem associated with the serviceability limit state, the procedure should not be linked to ultimate limit state parameters such as f_{fu}.

A second observation noted by Bischoff [4] refers to the definition of β_d. FRP-reinforced concrete beams and one-way slabs do not have reduced tension stiffening because of the FRP reinforcement properties but because of the tension-stiffening component in the original Branson's equation ($I_e = I_g - [I_g - I_{cr}] [1-(M_{cr}/M_a)^4]$),

which is very large for FRP-reinforced concrete members. At crack locations, the concrete carries essentially zero tension. Between cracks, however, the concrete participates in resisting tensile stress because of bond between the reinforcement and the concrete. This effect is often referred to as tension stiffening and is taken into account with the effective second moment of area [5].

2 Experimental program

Three concrete slabs were constructed and tested. The slabs had the same cross sectional dimensions, b = 500 mm and h = 150 mm (Fig. 1) with a total length of 2800 mm. They were reinforced longitudinally using GFRP rebar of 12.7 mm nominal diameters (d_b). No stirrups were provided in the test specimens. The reinforcement ratio (ρ_f), the clear bar spacing (***cbs***) and GFRP arrangement were all varied. The concrete cover (**c**) on both side of the specimens was kept constant (50 mm) in all test slabs. The reinforcement details for the test slabs are given in Table 1.

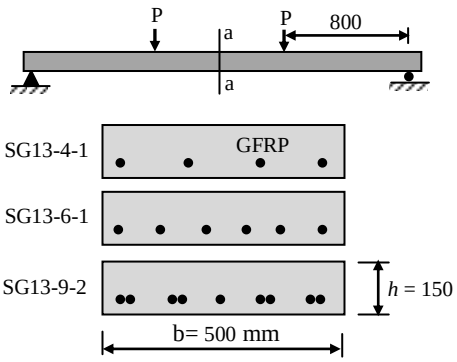

Fig.1. Slab cross sections (a-a).

Table 1. GFRP reinforcement in test Specimens.

Slab	Bars	d_b mm	ρ_f %	c mm	cbs mm	GFRP arrangement
SG13-4-1	4	12.7	0.82	20	116	Single bar
SG13-6-1	6	12.7	1.23	20	65	Single bar
SG13-9-2	9	12.7	1.84	20	72	Bundled bar

Figure 2 shows the mechanical loading test set-up. In this test, the slab specimens were simply supported with a span of 2400 mm and a shear span of 800 mm. All concrete specimens were subjected to two concentrated loads, each applied at one third of the 2400 mm tested length. Strain gauges, 5 mm long type BFLA-5-3 [6], were bonded longitudinally onto the rebars of each test specimen. They were positioned halfway between two spiral wraps. Each rebar had one 5 mm strain gauge placed at midpoint of the GFRP rebar. The idea of using strain gauges was to monitor the movements of the GFRP rebars under applied loads.

Fig. 2. Mechanical loading test set-up.

2.1 Material properties

Glass Fiber Reinforced Polymer rebar (Type E) was selected because it was the most widely used in the composite industry. The GFRP rebars were made of continuous longitudinal E-glass fibers bound together with a vinyl ester resin matrix with an external sand coating [1]. The bars contained 70% fiber by volume. These bars had a surface deformation called 'wrapped and sand coating design'. The 'wrapped' refered to the spiral glass fibers that were twisted around the bar. This decreases the amount of transverse thermal expansion and increases the mechanical interlock with the concrete. The bar was also sand coated to increase the friction and interlocking bond. The longitudinal modulus of elasticity of GFRP, E_g is 40.8 GPa, and its ultimate strength, f_{fu} is 690MPa for 12.7 mm bar diameters.

The concrete mix design had the following properties: a water-cement ratio of 0.55: 355 kg/m^3 ordinarily Portland cement, 195 kg/m^3 water, 724 kg/m^3 fine aggregate and 1086 kg/m^3 coarse aggregate (maximum 20 mm diameter). No super plasticizer was added to increase the concrete workability. The measured average compressive strength of the concrete used ranged from 44 to 55 MPa and the average splitting strength ranged from 2.7 to 3.3 MPa.

2.2 Testing procedure

The slab specimens were tested up to failure as simply supported slabs at room temperature. The test was carried out under load control. Each test specimen was subjected to increasing load increments at the rate of 3 kN per minute, until failure. The applied loads were measured using a load cell attached to the hydraulic jack. After each load increment, the crack pattern was marked and the surface crack width and spacing were measured. Specimens were instrumented with LVDTs at mid span to monitor the vertical deflection. All measurements were regularly recorded at 20 minute intervals.

3 PRESENTATION OF RESULTS

3.1 Cracking moment

The ACI predicted and experimental cracking moments M_{cr} of the GFRP reinforced concrete slabs are presented in Table 2. The experimental M_{cr} was recorded at the first visual crack. The theoretical M_{cr} was calculated based on the tensile strength of the concrete obtained from: (**1**) the tensile splitting test (f_{ct}; experimentally determined) and; (**2**) the modulus of rupture $f_r = 0.62\sqrt{f_c}$ (f_c is cylinder

compressive strength of concrete, MPa).The M_{cr} value at which first cracking occurs is

$$M_{cr} = 2f_r I_g / h \quad (3)$$

Table 2. Predicted and experimental cracking moments.

Slab	f_{cu} (MPa)	f_{ct} (MPa)	f_r (MPa)	M_{cr} (kN m) Exp.	ACI 440 (1)	ACI 440 (2)
SG13-4-1	43.7	2.7	3.7	5.2	5.1	6.9
SG13-6-1	55.2	3.3	4.1	4.8	6.2	7.7
SG13-9-2	49.2	3.2	3.9	5.6	6.0	7.3

It can be seen from Table 2 that the ACI M_{cr} using f_{ct} reasonably predicted (within -2% to 29%) the experimental M_{cr}. On the other hand, the ACI M_{cr} values using f_r overestimated (by 30% to 60%) the slab M_{cr} values. The difference in the concrete tensile strength between f_{ct} and f_r values was that the f_r equation was empirically derived using a statistical fit of variable whereas f_{ct} was experimentally derived from the properties of concrete used in this investigation only. It can be concluded tha as expected the f_{ct} values appeared to represent the experimental results much more closely. The difference in the ACI M_{cr} resulting from the two values (f_{ct} and f_r) was considered sufficient and hence the ACI M_{cr} resulting from f_{ct} was used in the theoretical predictions.

3.2 Load-deflection curves up to ultimate load

The characteristics of GFRP reinforcement include high strength, low specific gravity and corrosion resistance. However, despite the many advantages in mechanical and chemical properties, GFRP reinforcement possesses a relatively low elastic modulus of elasticity compared with that of steel. As a consequence, for GFRP reinforced sections, larger deflections and crack widths are expected than the ones obtained from equivalent steel reinforced sections for the same load.

Figure 3 shows the load-deflection curves up to maximum load generated by the ACI 440 and the corresponding measured curves for slabs SG13-4-1, SG13-6-1 and SG13-9-2. The experimental deflection shown was measured at midspan and the predicted deflections (Δ) were calculated using Eq. (4).

$$\Delta = [(Pa)/(24E_cI_e)]\ (3L^2-4a^2) \quad (4)$$

Where P is the applied load (kN); a is shear span, mm; E_c is modulus of elasticity of concrete, MPa; L is span length, mm.

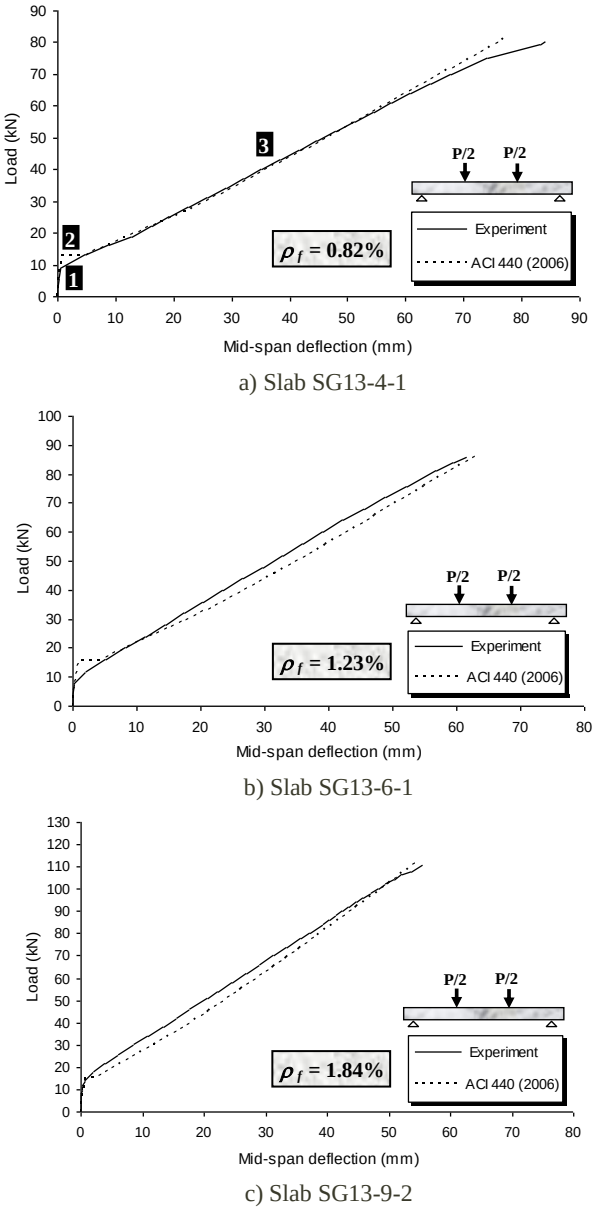

Fig. 3. Load versus deflection for slabs.

It can be seen from Figure 3 that the ACI 440 approach appeared to predict the behaviour of slab SG13-4-1with reinforcement ratio ρ_f = 0.82% throughout the range of post cracking up to ultimate load reasonably well (although it showed a larger deflection at a load of 75 kN and above; this was possibly due to the increased formation of internal cracks around the bars which reduce the tension stiffening of the concrete). On the other hand, the ACI deflections overestimated (by 1% to 15 % and by 1% to 73%) the experimental deflection of slabs SG13-6-1and SG13-9-2 at loads ranging from 20 to 86 kN and 22 to 106 kN, respectively.

The difference in the deflections between the predicted and measured values was due to the effect of the second moment of area I_e of each slab. This effect appeared to be small with slab SG13-4-1 reinforced with low ρ_f, whilst it was larger with heavily reinforced slabs (SG13-6-1and SG13-9-2 were reinforced with ρ_f = 1.23% and 1.84%, respectively). It therefore appears that the

ACI approach for predicating the effect of second moment of area I_e is more suitable for lightly reinforced slabs (less than 1%).

To confirm the I_e effect on deflection, the values of I_e determined using ACI 440 Eq. (1) are plotted against load for the slab SG13-6-1as shown in Figure 4. Slab SG13-6-1(Fig. 4) was taken as a case study. They are plotted along with the experimental values determined using the following equation based on Eq. (4):

$$I_{e(exp)} = [(P_{exp}\, a)/(24E_c\, \Delta_{exp})]\ (3L^2-4a^2) \quad (5)$$

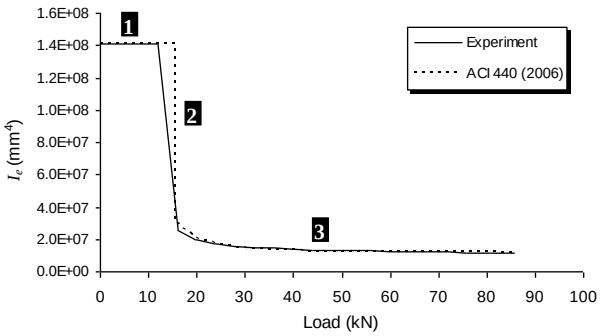

Fig. 4. I_e versus load for slab SG13-6-1.

Changes in deflection as a function of load are explained by considering three stages as labelled on Figures 3 and 4.

Case 1: when a section is uncracked, its second moment of area I is equal to the gross second moment of area I_g. When the applied moment M_a exceeds M_{cr}, cracking occurs, causing a reduction in the stiffness of the slab section; the second moment of area is then equal to I_e throughout the range of post cracking up to ultimate load. As Figure 4 shows, the experimental I_e dropped sharply before the ACI I_e. This was because slab SG13-6-1 had a lower experimental cracking moment than the predicted value (see Table 2). The same can be observed for the other slab specimens listed in Table 2.

Case 2: as shown in Figure 3, the slope of the load-deflection curves changes after cracking and this correlates to a decrease in I_e (Fig. 4). It is also noted that the slope of the load versus deflection curves of the slabs calculated from the ACI 440 changes sharply after cracking; this correlates to a sharp decrease in I_e due to smaller values of β_d (see Eq. 1). The values of β_d are 0.17, 0.22 and 0.35 for slab SG13-4-1, SG13-6-1and SG13-9-2, respectively. This was because the slab specimens were provided with different reinforcement ratios (0.82, 1.23 and 1.84%, respectively).

Case 3: the test results indicate that once the concrete has cracked, the slab deflections depend on the loading rate (Fig. 3). As mentioned before, the ACI deflection overestimated the experimental deflection of slab SG13-6-1. This was because the predicted I_e values were lower than the experimental values. This can be explained by considering the elastic deflection equation (4). From this equation it can be seen that when the effective moment of area I_e is smaller the induced deflection will be larger. This explanation can also be applied to slabs SG13-4-1 and SG13-9-2.

It can be concluded that the deflections of GFRP slabs can generally be predicted by elastic deflection equation and using the effective second moment of area I_e provided by the ACI 440. The predictions are better for lower reinforcement ratios (i.e. <1%).

3.3 Ultimate moment capacity

The theoretical moments computed using the ACI 440 equation (Eq. 6) and the experimental moments of the control specimens are presented in Table 3. The ratio of the predicted to measured moments is also shown in Table 3.

$$M_n = \rho_f\, f_f\, [1-0.59\, (\rho_f\, f_f / f_c)]\, bd^2 \quad (6)$$

$$f_f = n_f\, M\, (d-kd)/\, I_{cr} \quad (7)$$

Where ρ_f is FRP reinforcement ratio; f_f is stress in the FRP reinforcement in tension, MPa; f_c is cylinder compressive strength of concrete, MPa; b is width of rectangular cross section, mm; d is distance from extreme compression fibre to centroid of tension reinforcement; $n_f = E_f/E_c$; applied moment, kN m and k is the ratio of the depth of the neutral axis to the reinforcement depth. Note that the strength reduction factor ϕ was set to 1.

As shown in Table 3, the experimental moments M_{exp} are generally equal to or lower than the ACI unfactored design moment M_n which satisfies the ACI condition, i.e. $M_n \geq M_{exp}$.

Table 3. Predicted and experimental ultimate moments.

Slab	d mm	f_c MPa	ρ_f (%)	Moment (kN m)		
				Exp.	ACI	Ratio
SG13-4-1	124	35.2	0.82	32	32	1.00
SG13-6-1	124	44.0	1.23	34	41	1.21
SG13-9-2	124	39.2	1.84	44	46	1.05

3.4 Failure mode

Table 4 presents the actual reinforcement ratio ($\rho_f = A_f / b\, d$) for each test specimen, as well as the corresponding balanced reinforcement ratios (ρ_{fb}) according to ACI 440. It is important to note that crushing failure in GFRP slabs is assumed when concrete reached its ultimate compressive strain, ε_{cu}= 0.003. If the $\rho_f > \rho_{fb}$, concrete crushing governs. However, a shear failure was observed in all test specimens as shown in Figure 5. Although the test specimens had a GFRP reinforcement ratio ρ_f above the balanced ratio ρ_{fb} (Table 4), this shear failure does not satisfy the failure mode predicted by ACI-440 (when $\rho_f > \rho_{fb}$, concrete crushing governs). However, a shear failure mode was not surprising due to the absence of links in the shear spans.

All the test specimens were checked for adequacy of section for shear capacity, and it was found that the shear contribution of the concrete itself is inadequate ($V_u > V_c$).

Table 4 Reinforcement ratios and modes of failure.

Slab	ρ_{fb} (%)	ρ_f (%)	Comments	Failure Mode
SG13-4-1	0.55	0.82	Over-reinforced	Shear failure
SG 13-6-1	0.66	1.23	Over-reinforced	Shear failure
SG13-9-2	0.62	1.84	Over-reinforced	Shear failure

Fig. 5. Shear failure of SG13-9-2 under mechanical load.

3.5 Crack width prediction

The width of cracks in flexural members depend on the crack spacing, the quality of bond between the concrete and reinforcing bars, and above all, the strain in the reinforcement [7]. For a specified strain in the reinforcement, the width of crack can vary substantially from member to member, depending on parameters such as load duration or repetition of loading, shape and dimensions of the cross section and concrete cover. To control the width of cracks in concrete sections reinforced with GFRP and subjected to bending, it is necessary to limit the stress in the reinforcement to a relatively small fraction of the ultimate strength [8].

An advantage of glass FRP rebars over steel reinforcement is that there is no risk of corrosion. Thus, crack widths have to be controlled to satisfy the requirements of appearance and type of use. The ACI Committee 440 limits crack widths to 0.5 and 0.7mm for exterior and interior exposure, respectively.

3.5.1 *Tensile stress in GFRP bars*

Figure 6 shows the experimental and theoretical stresses in GFRP reinforcement in tension provided by the ACI-440. The tensile stress (f_f) of the GFRP bar obtained from the test results is based on the average of two recorded strains (ε_{exp}) multiplied by the elastic modulus (E_f) of GFRP, ($f_f = \varepsilon_{exp}$ x E_f), whilst the ACI stress was calculated according to Eq. (7).

As can be seen from Figure 6, the ACI stress f_f (required for crack width prediction) overestimated (by 38% to 11% at a load of about 30 to 80 kN, respectively) the experimental f_f of slab SG13-6-1. On the other hand, at lower loads (i.e. 30 kN) the ACI f_f overestimated the experimental f_f by 49%.

The over-predicted stress by the ACI 440 was thought to be due to the assumption that the depth of neutral axis (N.A) is constant, post cracking ($M > M_{cr}$). This is incorrect as the N.A. is known to vary. Also ACI uses the cracked second moment of area I_{cr} (Eq. 7) instead of the effective second moment of area I_e (i.e. I_e represents the second moment of area for $M > M_{cr}$. As $I_{cr} < I_e$, this will predict a greater f_f .

Where the moment exceeds M_{cr}, the concrete in tension is expected to fail at the outer tension fibres and the cracks propagate towards the neutral axis. The average spacing between cracks reduces and the average crack width increases with increase in moment M beyond M_{cr}. In a beam subjected to a sufficient constant moment where $M > M_{cr}$, theoretically the entire beam could be fully cracked on the tension side of the neutral axis (stabilized cracking patterns).

However, the concrete in between the cracks still resists some tension, and this is reflected in a reduction in tensile strain in the reinforcement, a lowering of the neutral axis and a fluctuation in the bond stress as well as a reduction in curvature. The tensile strain in the reinforcement midway between the cracks is lower than that strain at the crack location. Therefore, the stress f_f to be considered may be reasonably based on the mean stress, rather than the stress at the crack location (which is higher). The use of a higher value of f_f results in a more conservative (larger) estimate of the crack width.

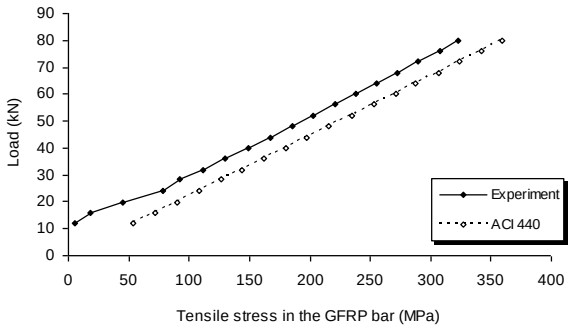

Fig. 6. Load versus stress in the GFRP bars (SG13-6-1).

3.5.2 *Crack width*

Crack widths in GFRP reinforced concrete members, as mentioned above, are expected to be larger than those in steel reinforced concrete members. For GFRP reinforced members, ACI 440 allows crack widths to be calculated as:

$$w = 2(f_f/E_f)\,\beta\,k_b\,\sqrt{[d_c^2 + (s/2)^2]} \quad (8)$$

where E_f is longitudinal modulus of elasticity of FRP reinforcement, MPa; β is ratio of the distance from the neutral axis to extreme tension fibre to the distance from the neutral axis to the centre of the tensile reinforcement; k_b is bond-dependent coefficient; d_c thickness of the concrete cover measured from extreme tension fibre to centre of bar, mm and s is bar spacing, mm.

Figures 7 and 8 show the load versus maximum crack width obtained from experimentally and from the ACI results for slabs (SG13-6-1and SG13-9-2). The slabs were provided with the same bar diameter (13 mm) and

concrete cover (20 mm) but with different reinforcement ratios (ρ_f = 1.23% and 1.84%, respectively).

It appears from Figures 7 and 8 that as ρ_f increases crack width predictions improve. Also, at a load where σ_f = 15%f_f the code over predicted crack widths by 53% and 16% for the slab SG13-6-1 and SG13-9-2, respectively. In each case the predictions improve with increased load.

The difference between the ACI crack width prediction and the experimental values was thought to be due to the over predicted stress f_f generated by the ACI approach (Eq. 7) and the conservative k_b value of 1.4. It was noted that the increase in experimental crack width was not linear ('zig-zagging shape'). This may be attributed to the initiation of new cracks at other locations a long the slab length.

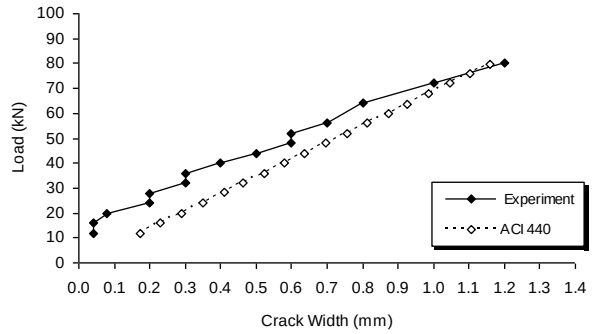

Fig. 7. Load versus crack width for Slab SG13-6-1.

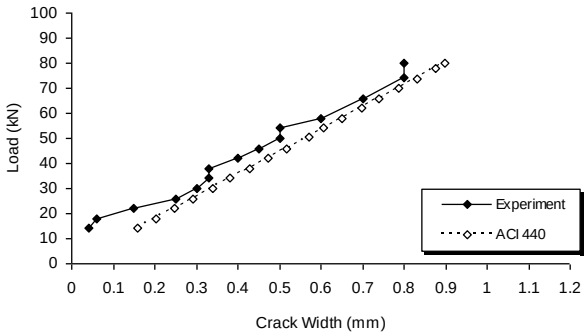

Fig. 8. Load versus crack width for Slab SG13-9-2.

4 Conclusions

A discussion of the ACI 440 approaches in comparison with the test results can lead to the following conclusions:

1. The ACI 440 equations for predicting the cracking moment, using the concrete tensile strengths determined experimentally predicted reasonably well the experimental values obtained in this investigation for the GFRP reinforced slab. On the other hand, the ACI predicted moment based on the modulus of rupture f_r, overestimated the experimental cracking moment.
2. The maximum experimental moments M_{exp} were equal to or lower than the ACI unfactored design moment M_n which meets the ACI 440 requirement, i.e. $M_n \geq M_{exp}$.
3. The deflections of the GFRP reinforced slabs were well predicted for lightly reinforced slabs (less than 1%) using the I_e equation provided by ACI 440. On the other hand, the ACI deflections overestimated the experimental deflection of slabs SG13-6-1 and SG13-9-2 reinforced with ρ_f = 1.23% and 1.84%, respectively.
4. The predicted stress required for crack width prediction overestimated the stress of the experimental results. The reasons for the over-predicted stress by the ACI 440 were thought to be due to the assumption that the depth of neutral axis is constant, post cracking ($M > M_{cr}$), This is incorrect as the N.A. is known to vary. Also ACI uses the I_{cr} instead of the I_e.
5. The predicted crack widths using ACI Eq. (8) were wider, in general, but compared reasonably well with the measured ones in slabs reinforced with higher reinforcement ratios (i.e. 1.84%).

References

1. Hughes Brothers, Inc. (2002). Aslan 100 Fiber glass Rebars. Technical Data: www.hughesbros.com.
2. ACI Committee 440 (ACI 440.1R-06), (2006). Guide for the Design and Construction of Structural Concrete Reinforced with FRP Bars. *American Concrete Institute*.
3. Ospina, C.E. and Nanni, A. (2007). Current FRP-Reinforced Concrete Design Trends in ACI 440.1R. *In: the 8th international symposium on fiber-reinforced polymer reinforcement for concrete structures*, FRPRCS-8. Patras, Greece, July 16-18, 2007.
4. Bischoff, P.H. (2007). Rational model for calculating deflection of reinforced concrete beams and slabs. *Canadian Journal of Civil Engineering*, **34** (8), pp. 992-1002.
5. Bischoff, P.H. and Scanlon, A. (2007). Effective moment of inertia for calculating deflections of concrete members containing steel reinforcement and fiber-reinforced polymer reinforcement. *ACI Structural Journal*, **104** (1), pp. 68-75.
6. Tokyo Sokki Kenkyujo Co., Ltd. (TLM). TML Strain Gauge Users Guide (TML PAM E-101P). Tokyo. http://www.tokyosokki.co.jp/e/.
7. Wang, C. K. and Salmon, C. G. (1992). *Reinforced Concrete Design*. 5th Edition. New York: Harper Collins, pp. 1030.
8. Newhook, J., Ghali, A. and Tadros, G. (2002). Concrete flexural members reinforced with fiber reinforced polymer: design for cracking and deformability. *Canadian Journal of Civil Engineering*, 29, pp 125-134.